

Target recognition using HRR profile-based incoherent SAR (InSAR) image formation

Nicholas A. O'Donoghue^{*ab}, Walter S. Kuklinski^a, Constantine Arabadjis^a

^aThe MITRE Corp., E532 Signal Processing, 202 Burlington Road, Bedford, MA USA 01730-1420;

^bECE Dept., Carnegie Mellon University, HH 1111, 5000 Forbes Ave, Pittsburgh, PA USA 15213

ABSTRACT

Feature-aided target verification is a challenging field of research, with the potential to yield significant increases in the confidence of re-established target tracks after kinematic confusion events. Using appropriate control algorithms airborne multi-mode radars can acquire a library of HRR (High Range Resolution) profiles for targets as they are tracked. When a kinematic confusion event occurs, such as a vehicle dropping below MDV (Minimum Detectable Velocity) for some period of time, or two target tracks crossing, it is necessary to utilize feature-aided tracking methods to correctly associate post-confusion tracks with pre-confusion tracks. Many current HRR profile target recognition methods focus on statistical characteristics of either individual profiles or sets of profiles taken over limited viewing angles. These methods have not proven to be very effective when the pre- and post- confusion libraries do not overlap in azimuth angle.

To address this issue we propose a new approach to target recognition from HRR profiles. We present an algorithm that generates 2-D imagery of targets from the pre- and post-confusion libraries. These images are subsequently used as the input to a target recognition/classifier process. Since, center-aligned HRR Profiles, while ideal for processing, are not easily computed in field systems, as they require the airborne platform's center of rotation to line up with the geometric center of the moving target (this is impossible when multiple targets are being tracked), our algorithm is designed to work with HRR profiles that are aligned to the leading edge (the first detection above a threshold, commonly referred to as Edge-Aligned HRR profiles).

Our simulated results demonstrate the effectiveness of this method for classifying target vehicles based on simulations using both overlapping and non-overlapping HRR profile sets. The algorithm was tested on several test cases using an input set of .28 m resolution XPATCH generated HRR profiles of 20 test vehicles (civilian and military) at various elevation angles.

Keywords: Radar imaging, HRR, Target Recognition, Feature-Aided Tracking, Incoherent SAR

1. INTRODUCTION

There is a significant body of research devoted to the methods for obtaining and maintaining long term continuous track on targets of interest with radar systems [1,5,6,7,9]. With proper control methods, multi-mode radars can maintain tracks on targets of interest using Ground Moving Target Indicator (GMTI) modes [2], while gathering a set of HRR profile measurements whenever new azimuth angles to the target are presented. A significant drawback of Doppler-based GMTI radar tracking systems is that targets are lost when their radial velocity drops below the MDV (Minimum Detectable Velocity). Presumably, if a vehicle resumes its rate of travel at some later point in time it would be necessary to determine if the new track should be considered an extension of the original target track. This is commonly referred to as a confusion event.

Confusion events can be as simple as a single track being lost and regained at some later time, or they may include multiple vehicles simultaneously (i.e. two vehicles approaching an intersection). It is imperative that reliable methods of target recognition be employed to ensure that consistent tracks are maintained on target vehicles, even when there are several tracks involved in the confusion event, this can be viewed as an m-ary classification problem.

* odonoghue@mitre.org; phone: 1.412.268.7103; fax: 1.412.268.3890; mitre.org

Most current HRR profile recognition approaches focus on methods that directly compare profile statistics [1,5,6,7] (such as electronic length vs. azimuth) in order to determine if two sets of HRR profiles were generated from the same target. The most significant challenge to these approaches is that HRR profiles are statistically independent for even a small degree of azimuth separation. There is some dispute over exactly how much correlation there is between HRR profiles at separate azimuth angles (one study claims a complete loss of correlation after 0.2 degrees, while another shows significant similarity even after 5 degrees of separation) [6], but what is clear is that HRR profiles that are separated by modest azimuth angles have little statistical similarity. This decorrelation limits direct HRR profile comparison methods to those cases where an overlap of azimuth angles exists.

For the case where two sets of profiles do not have support over a common range of azimuth angles, current classification methods are unsatisfactory. This work attempts to overcome that limitation by performing comparison on target imagery derived from the HRR profiles instead of direct comparison on the profiles themselves. We analyze the factors that influence the structure HRR profiles, and through our analysis we demonstrate a reliable imaging algorithm for partial libraries of leading edge-aligned HRR profiles. We call this approach Edge-Aligned Incoherent SAR (EA InSAR). While it would be ideal to work with HRR profiles aligned to the geometric center of the target, which would require the airborne platform to match its center of rotation to the target's geometric center. This would be extremely difficult in single target cases and impossible when multiple targets are tracked. Edge-Aligned HRR profiles, on the other hand, are easy to obtain and require no modifications of the airborne platform's flight path.

The algorithm that we present has been tested using XPATCH generated HRR profiles for 20 different vehicles (a mix of civilian and military craft). The list of test vehicles is presented in the Appendix. Section 2 provides the assumed geometrical framework for our model. Section 3 provides a review of HRR profile structure. Section 4 describes the method used to estimate overall target size, a necessary pre-cursor to our imaging process, which is formulated in Section 5. Our target recognition method is described in Section 6. Section 7 contains simulation results, with our conclusion found in section 8.

2. SYSTEM GEOMETRY

2.1 Differential Range

In the assumed system geometry, an airborne radar platform radiates a given ground patch from a very large stand-off distance, and maintaining tracks on various moving targets. From these tracks, and HRR measurements, HRR profile libraries (amplitude vs. range for various azimuth angles) are constructed

The scatterers that comprise targets of interest are labeled as points 1 through N and the k^{th} scatterer having reflectivity α_k . Note the layout as shown in Figure 1. The range between the radar platform and the k^{th} scatterer is $R_k = |\vec{\mathbf{R}}_k|$, and the range from the origin to each scatterer is $r_k = |\vec{\mathbf{r}}_k|$.

We note that the range R_k can be calculated with

$$\begin{aligned} R_k &= |\vec{\mathbf{R}}_k| = |\vec{\mathbf{r}}_k - \vec{\mathbf{r}}_0| = \sqrt{r_k^2 - 2r_0r_k \cos \gamma_k + r_0^2} \\ &= r_0 \sqrt{1 - 2(r_k/r_0) \cos \gamma_k + (r_k/r_0)^2} \end{aligned} \tag{1}$$

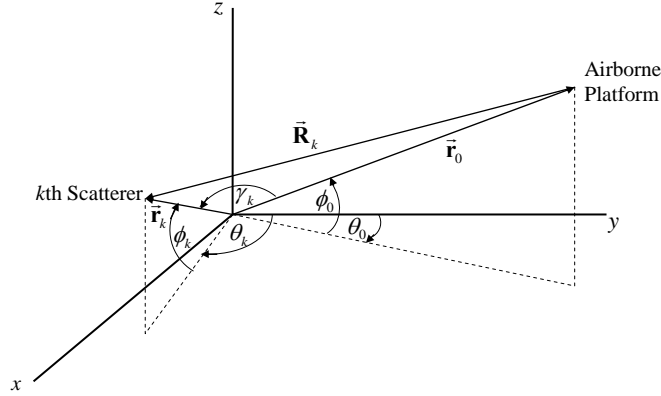


Figure 1 - Physical Layout

By taking the 1st-Order Taylor Series approximation for $\sqrt{1 - 2au + u^2}$ around $u=0$, and noting that

$$\cos \gamma_k = \cos \phi_0 \cos \phi_k \cos(\theta_k - \theta_0) + \sin \phi_0 \sin \phi_k, \quad (2)$$

we can express the differential range as:

$$R_k \approx r_0 - r_k \cos \gamma_k = r_0 - r_k (\cos \phi_0 \cos \phi_k \cos(\theta_k - \theta_0) + \sin \phi_0 \sin \phi_k). \quad (3)$$

We define the differential range between the radar platform and the k^{th} scatterer as

$$\Delta R_k = R_k - r_0 = -r_k (\cos \phi_0 \cos \phi_k \cos(\theta_k - \theta_0) + \sin \phi_0 \sin \phi_k). \quad (4)$$

Thus, our calculations for differential range (estimated to the 1st Order) are independent of the radar platform's standoff range to the target. Figure 2 shows two scatterers, and their differential ranges. The graphic is not drawn to scale as r_0 is typically much larger than it is shown here. It is clear from the graph, however, that as $r_0 \rightarrow \infty$, $-\Delta R_1$ and $-\Delta R_2$ approach the projections of r_1 and r_2 onto the radial line from the origin to the platform.

2.2 Edge Alignment

We sort the set of N differential ranges and notate them as $\Delta R_{(1)}, \Delta R_{(2)}, \dots, \Delta R_{(N)}$, such that

$$\begin{aligned} \Delta R_{(1)} &= \min(\Delta R_1, \Delta R_2, \dots, \Delta R_N), \\ \Delta R_{(N)} &= \max(\Delta R_1, \Delta R_2, \dots, \Delta R_N). \end{aligned} \quad (5)$$

It is clear that $\Delta R_{(1)}$ is the differential range of the scatterer nearest to the Radar platform, and $\Delta R_{(N)}$ is the differential range of the scatterer farthest from the platform. The edge-aligned differential range for each scatterer is defined as:

$$\delta R_k = \Delta R_k - \Delta R_{(1)}, \quad k = 1, 2, \dots, N. \quad (6)$$

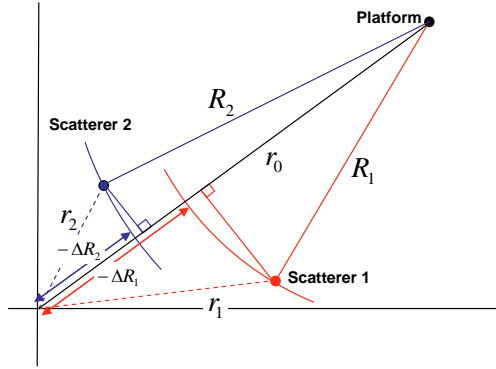


Figure 2 - Differential Range

3. HRR PROFILES

In this section, we first analyze the structure of HRR profiles and develop a matrix representation for our model.

3.1 Description

The HRR profile is the observed amplitude (power) versus the differential range ΔR for a given location of the platform and the scatterers. The differential range ΔR is discretized as a sequence of L consecutive range bins, labeled $\mathfrak{R}_1, \mathfrak{R}_2, \dots, \mathfrak{R}_L$, each of width w . We denote this HRR profile as $h(\mathfrak{R}_i; \theta_0, \phi_0, \mathbf{s}, \boldsymbol{\alpha})$, where the N by 3 scatterer location matrix \mathbf{s} defines the location of the N scatterers and $\boldsymbol{\alpha}$ is a vector containing the N reflectivities:

$$\mathbf{s} = \begin{bmatrix} r_1 & \theta_1 & \phi_1 \\ \vdots & \vdots & \vdots \\ r_N & \theta_N & \phi_N \end{bmatrix}, \quad \boldsymbol{\alpha} = \begin{bmatrix} \alpha_1 \\ \vdots \\ \alpha_N \end{bmatrix}. \quad (7)$$

The value of $h(\mathfrak{R}_i; \theta_0, \phi_0, \mathbf{s}, \boldsymbol{\alpha})$ is the sum of the reflectivities in the i^{th} bin \mathfrak{R}_i . For example if there are N scatterers present at ranges $\Delta R_1, \Delta R_2, \dots, \Delta R_N \in \mathfrak{R}_i$ with reflectivities $\alpha_1, \alpha_2, \dots, \alpha_N$, then the HRR profile at that range bin is given by:

$$h(\mathfrak{R}_i; \theta_0, \phi_0, \mathbf{s}, \boldsymbol{\alpha}) = \sum_{\substack{k=1 \\ \Delta R_k \in \mathfrak{R}_i}}^N \alpha_k, \quad i = 1, 2, \dots, L. \quad (8)$$

Writing this equation in matrix form, yields L linear equations (one for each range bin):

$$\mathbf{h}(\theta_0, \phi_0, \mathbf{s}, \boldsymbol{\alpha}) = \begin{bmatrix} h(\mathfrak{R}_1; \theta_0, \phi_0, \mathbf{s}, \boldsymbol{\alpha}) \\ \vdots \\ h(\mathfrak{R}_L; \theta_0, \phi_0, \mathbf{s}, \boldsymbol{\alpha}) \end{bmatrix} = \mathbf{U}(\theta_0, \phi_0, \mathbf{s}) \boldsymbol{\alpha}, \quad (9)$$

where the assignment matrix $\mathbf{U}(\theta_0, \phi_0, \mathbf{s})$ is an L by N matrix of zeros and ones, the i, k^{th} element of $\mathbf{U}(\theta_0, \phi_0, \mathbf{s})$ is given by

$$u_{ik}(\theta_0, \phi_0, \mathbf{s}) = \begin{cases} 1 & \Delta R_k \in \mathfrak{R}_i \\ 0 & \text{otherwise} \end{cases}. \quad (10)$$

3.2 Structure of the Assignment Matrix

The assignment matrix $\mathbf{U}(\theta_0, \phi_0, \mathbf{s})$ assigns a scatterer to a range bin, as given by Eq. (10). Let \mathbf{u}_i^r denote the i^{th} row and \mathbf{u}_i^c denote the i^{th} column of $\mathbf{U}(\theta_0, \phi_0, \mathbf{s})$.

Every scatterer is assigned to one, and only one range bin. A range bin may contain none or several scatterers. If the k^{th} scatterer falls into the i^{th} range bin, then the i^{th} element of \mathbf{u}_k^c is one and all other elements are zero. Thus every column vector $\mathbf{u}_k^c, k = 1, 1, \dots, N$ contains one and only one element that is one, all others are zero. This implies that

$$\begin{aligned} \mathbf{u}_i^{c\top} \mathbf{u}_i^c &= 1, \\ \mathbf{u}_i^{c\top} \mathbf{u}_j^c &= \begin{cases} 1 & \Delta R_i, \Delta R_j \text{ are in the same range bin} \\ 0 & \text{otherwise} \end{cases}. \end{aligned} \quad (11)$$

If n_i is the number of scatterers that fall into range bin i then

$$n_i = \mathbf{u}_i^r \mathbf{u}_i^{r\top}. \quad (12)$$

Furthermore since every column has only one element that is one and all others are zero it follows that no two rows have ones in the same position. This implies that

$$\mathbf{u}_i^r \mathbf{u}_j^{r\top} = \begin{cases} n_i & i = j \\ 0 & i \neq j. \end{cases} \quad (13)$$

3.3 Edge Aligned HRR Profiles

When the differential ranges are aligned to the leading edge, we represent the shifted range bins as $\tilde{\mathfrak{R}}_1, \tilde{\mathfrak{R}}_2, \dots, \tilde{\mathfrak{R}}_L$, where $\tilde{\mathfrak{R}}_1$ covers the interval $[0, w)$, $\tilde{\mathfrak{R}}_2$ covers the interval $[w, 2w)$, and so on. Thus, instead of Eq. (8), we have:

$$\tilde{h}(\tilde{\mathfrak{R}}_i; \theta_0, \phi_0, \mathbf{s}, \boldsymbol{\alpha}) = \sum_{\substack{k=1 \\ \Delta R_k \in \tilde{\mathfrak{R}}_i}}^N \alpha_k, \quad i = 1, 2, \dots, L. \quad (14)$$

In matrix notation, that becomes

$$\tilde{\mathbf{h}}(\theta_0, \phi_0, \mathbf{s}, \boldsymbol{\alpha}) = \tilde{\mathbf{U}}(\theta_0, \phi_0, \mathbf{s}) \boldsymbol{\alpha}. \quad (15)$$

The observed edge-aligned HRR profile $\tilde{H}(\tilde{\mathfrak{R}}_i; \theta_0, \phi_0, \mathbf{s}, \boldsymbol{\alpha})$ is assumed to contain additive white noise in each bin, i.e.,

$$\tilde{H}(\tilde{\mathfrak{R}}_i; \theta_0, \phi_0, \mathbf{s}, \boldsymbol{\alpha}) = \tilde{h}(\tilde{\mathfrak{R}}_i; \theta_0, \phi_0, \mathbf{s}, \boldsymbol{\alpha}) + \tilde{\boldsymbol{\varepsilon}}_i. \quad (16)$$

Thus, the matrix notation is re-written as

$$\tilde{\mathbf{H}}(\theta_0, \phi_0, \mathbf{s}, \boldsymbol{\alpha}) = \tilde{\mathbf{U}}(\theta_0, \phi_0, \mathbf{s}) \boldsymbol{\alpha} + \tilde{\boldsymbol{\varepsilon}}. \quad (17)$$

We have a suite of HRR profile measurements at M different platform locations, noting each measurement as

$$\begin{aligned} \tilde{\mathbf{H}}_m &= \mathbf{H}(\theta_0(t_m), \phi_0(t_m), \mathbf{s}(t_m), \boldsymbol{\alpha}), \\ \tilde{\mathbf{U}}_m &= \mathbf{U}(\theta_0(t_m), \phi_0(t_m), \mathbf{s}(t_m)), \end{aligned} \quad (18)$$

then we can express the full suite as

$$\begin{bmatrix} \tilde{\mathbf{H}}_1 \\ \vdots \\ \tilde{\mathbf{H}}_M \end{bmatrix} = \begin{bmatrix} \tilde{\mathbf{U}}_1 \\ \vdots \\ \tilde{\mathbf{U}}_M \end{bmatrix} \boldsymbol{\alpha} + \begin{bmatrix} \tilde{\boldsymbol{\varepsilon}}_1 \\ \vdots \\ \tilde{\boldsymbol{\varepsilon}}_M \end{bmatrix}. \quad (19)$$

For notational simplicity, these matrices are referred to as

$$\tilde{\mathbf{H}} = \tilde{\mathbf{U}} \boldsymbol{\alpha} + \tilde{\boldsymbol{\varepsilon}}. \quad (20)$$

3.4 Constructing the Assignment Matrix

In order to image the target, we assume a dense two-dimensional grid of scatterers in the ground plane spanning a rectangle with dimensions x and y , and inter-element spacing equal to the range resolution of the HRR profiles. For the tests we conducted, x and y map out a 10m x 10m ground-plane grid and a resolution of 0.28m.

There is no additional information needed in order to construct HRR traces for the dense grid, but constructing traces for edge-aligned HRR profiles also requires detailed knowledge of the target's geometry. This is because the traces must be aligned to the nearest point on the target at each azimuth. To find that point we need a detailed target model. For simplicity, we assume that the vehicle is rectangular, and that all scattering points are in the ground plane. Given the assumed target shape and large standoff assumption all differential ranges are projections onto the azimuth vector. Consequently the only points needed for edge alignment are the four corners of the target, allowing us to use the simple dimension estimator in Section 4 to construct $\tilde{\mathbf{U}}$.

Thus, for each azimuth angle provided, we compute the assignment matrix \mathbf{U} for the full grid of scatterers, and perform edge-alignment based on the range bin of the nearest corner, to form $\tilde{\mathbf{U}}$.

4. TARGET SIZE ESTIMATION

4.1 LS Solution

Due to the nature of edge-aligned HRR traces, it is imperative that we estimate the size of the target first, so that when we construct the scatterer assignment matrix, we can properly perform the edge-alignment. If we assume that the electronic length of a target at a given azimuth is a good approximation for the physical length of the target at that azimuth, we can construct a relationship between electronic length (noted L_E), azimuth (θ_0), target length (L) and target width (W). To reference the previously noted coordinate system, we place the target such that the length is along the x -axis and width along the y -axis.

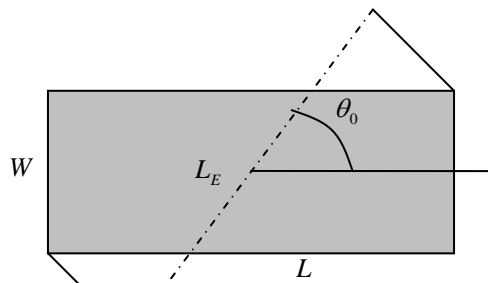


Figure 3 - Electronic Length

The projection of the nearest and farthest points onto L_E are valid because of the large standoff approximation. From Figure 4, we can draw the relationship

$$L_E = L|\cos \theta_0| + W|\sin \theta_0|. \quad (21)$$

However, the Electronic Length that we calculate from the HRR profiles is in the observation plane, so we must account for the elevation angle with

$$\tilde{L}_E = \frac{L|\cos \theta_0| + W|\sin \theta_0|}{\cos \phi}. \quad (22)$$

Next, we express this relationship, over the suite of azimuth angles for which we have HRR profile data, in matrix form:

$$\tilde{\mathbf{L}}_E = \begin{bmatrix} \frac{|\cos \theta_0(t_0)|}{\cos \phi_0} & \frac{|\sin \theta_0(t_0)|}{\cos \phi_0} \\ \vdots & \vdots \\ \frac{|\cos \theta_0(t_M)|}{\cos \phi_0} & \frac{|\sin \theta_0(t_M)|}{\cos \phi_0} \end{bmatrix} \begin{bmatrix} L \\ W \end{bmatrix} = \mathbf{A} \begin{bmatrix} L \\ W \end{bmatrix}. \quad (23)$$

To solve for the most likely vehicle dimensions, we compute the least-squares solution

$$\begin{bmatrix} \hat{L}_{LS} \\ \hat{W}_{LS} \end{bmatrix} = (\mathbf{A}^T \mathbf{A})^{-1} \mathbf{A}^T \tilde{\mathbf{L}}_E. \quad (24)$$

4.2 MMSE Solution

If the target classification problem is restricted to a domain of known vehicle types, we can use the corresponding length and width data for all candidate vehicles, noted \mathbf{L} and \mathbf{W} , respectively. Defining the mean-squared error as

$$MSE_n = \frac{(\tilde{W} - W_n)^2 + (\tilde{L} - L_n)^2}{2}. \quad (25)$$

Thus, we can estimate the vehicle dimensions \hat{L}_{MMSE} and \hat{W}_{MMSE} as:

$$\begin{aligned} k &= \arg \min (MSE_n) \\ \hat{L}_{MMSE} &= L_k \\ \hat{W}_{MMSE} &= W_k. \end{aligned} \quad (26)$$

4.3 Comparison

To verify the accuracy of our overall dimension estimates, we tested these algorithms on XPATCH generated data for 20 vehicles of varying size. The direct least-squares method results in a mean-squared error of 1.71m (see Figure 4), while the MMSE procedure resulted in a mean-squared error of 0.992m (see Figure 5).

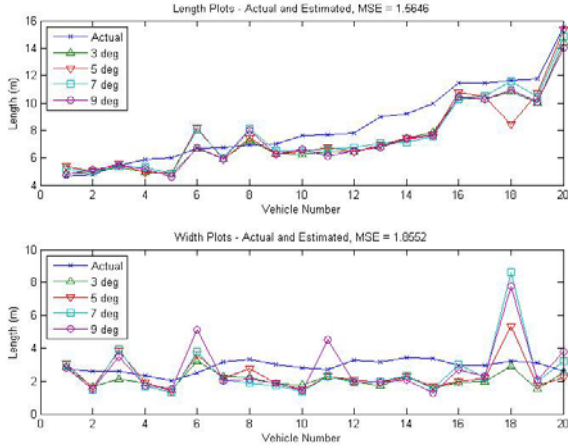


Figure 4 - LS Size Estimator

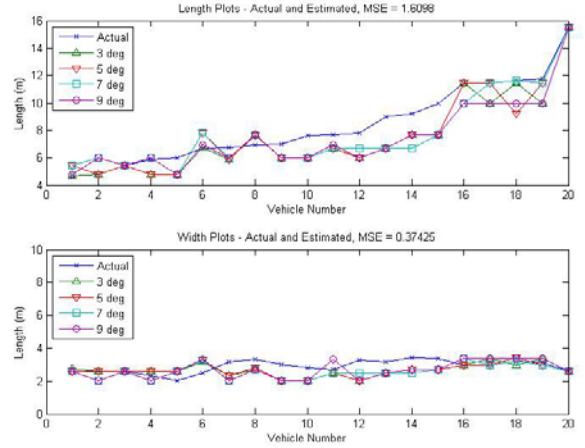


Figure 5 - MMSE Size Estimator

5. IMAGE FORMATION

Recall the matrix representation of the full suite of edge-aligned HRR profile measurements and the modeled assignment matrix:

$$\tilde{\mathbf{H}} = \tilde{\mathbf{U}} \boldsymbol{\alpha} + \tilde{\boldsymbol{\varepsilon}}. \quad (27)$$

We wish to estimate $\boldsymbol{\alpha}$ by a least-squares criterion. The total squared error is

$$\tilde{Q} = \tilde{\boldsymbol{\varepsilon}}^T \tilde{\boldsymbol{\varepsilon}} = (\tilde{\mathbf{H}} - \tilde{\mathbf{U}} \boldsymbol{\alpha})^T (\tilde{\mathbf{H}} - \tilde{\mathbf{U}} \boldsymbol{\alpha}). \quad (28)$$

$\hat{\boldsymbol{\alpha}}_{LS}$ is the least squares estimate and is that value of $\boldsymbol{\alpha}$ that minimizes \tilde{Q} . If $\tilde{\mathbf{U}}^T \tilde{\mathbf{U}}$ is a non-singular matrix, then $\hat{\boldsymbol{\alpha}}_{LS}$ is given by

$$\hat{\boldsymbol{\alpha}}_{LS} = (\tilde{\mathbf{U}}^T \tilde{\mathbf{U}})^{-1} \tilde{\mathbf{U}}^T \tilde{\mathbf{H}}, \quad (29)$$

If $\tilde{\mathbf{U}}^T \tilde{\mathbf{U}}$ is singular than the scatterer reflectivities are not resolvable and cannot be separately estimated, yielding an infinite set of possible least-squares solutions. Thus, it is imperative that the grid of scatterers to be estimated have an inter-element separation that is at least equal to the range resolution of the HRR profile.

Note that we can write

$$\tilde{\mathbf{U}}^T \tilde{\mathbf{U}} = M(\mathbf{I} + \tilde{\mathbf{D}}), \quad (30)$$

where the diagonal elements of the N by N symmetric matrix $\tilde{\mathbf{D}}$ are zero and off-diagonal elements are between 0 and 1 (indicating the percentage of azimuth angles for which a scatterer's range bin is shared by another scatterer), and M is the number of azimuth angles present in the data. Therefore, we can re-write Eq. (29) as

$$\hat{\boldsymbol{\alpha}}_{LS} = \frac{1}{M} (\mathbf{I} + \tilde{\mathbf{D}})^{-1} \tilde{\mathbf{U}}^T \tilde{\mathbf{H}}. \quad (31)$$

This requires the inversion of a very large matrix. Recall the series expansion for $1/(1+x)$,

$$(1+x)^{-1} = 1 - x + x^2 - x^3 + \dots = (1-x)(1+x^2+x^4+\dots). \quad (32)$$

Convergence of this series requires that x reside within the unit circle. The analogous form for square matrices is

$$(\mathbf{I} + \mathbf{X})^{-1} = \mathbf{I} - \mathbf{X} + \mathbf{X}^2 - \mathbf{X}^3 + \dots = (\mathbf{I} - \mathbf{X})(\mathbf{I} + \mathbf{X}^2 + \mathbf{X}^4 + \dots), \quad (33)$$

with the constraint that the eigenvalues of \mathbf{X} must reside within the unit circle. If convergence can be guaranteed, then the *modified least-squares* estimate of order p is

$$\begin{aligned} \hat{\mathbf{a}}_{MLS} &= \frac{1}{M} (\mathbf{I} - \tilde{\mathbf{D}} + \tilde{\mathbf{D}}^2 - \tilde{\mathbf{D}}^3 + \dots + \tilde{\mathbf{D}}^{2p}) \tilde{\mathbf{U}}^T \tilde{\mathbf{H}} \\ &= \frac{1}{M} (\mathbf{I} - \tilde{\mathbf{D}}) (\mathbf{I} + \tilde{\mathbf{D}}^2 + \tilde{\mathbf{D}}^4 + \dots + \tilde{\mathbf{D}}^{2p}) \tilde{\mathbf{U}}^T \tilde{\mathbf{H}}, \end{aligned} \quad (34)$$

with p chosen to balance the demands of accuracy and computation speed. Another approach to avoiding the inversion of $\tilde{\mathbf{U}}^T \tilde{\mathbf{U}}$ is to ignore $\tilde{\mathbf{D}}$, and obtain what we have called the *back-projection* estimate,

$$\hat{\mathbf{a}}_{BP} = \frac{1}{M} \tilde{\mathbf{U}}^T \tilde{\mathbf{H}}. \quad (35)$$

This estimate is essentially the modified least-squares estimate with order $p=0$. As it turns out, the back-projection estimate is suitable for imaging purposes, in that it provides reliable imagery, and does not require that our problem satisfy the singularity or eigenvalues constraints.

Figure 6 shows the center- and edge-aligned HRR Profiles for one of the test vehicles (a Mercedes Limousine). Back-projection imagery from a full 360° library is shown in Figure 7.

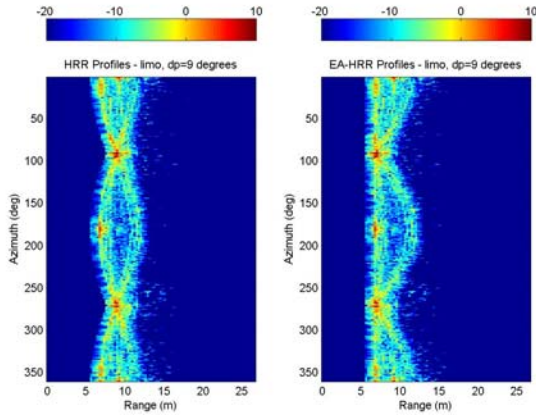


Figure 6 – Sample HRR Profiles

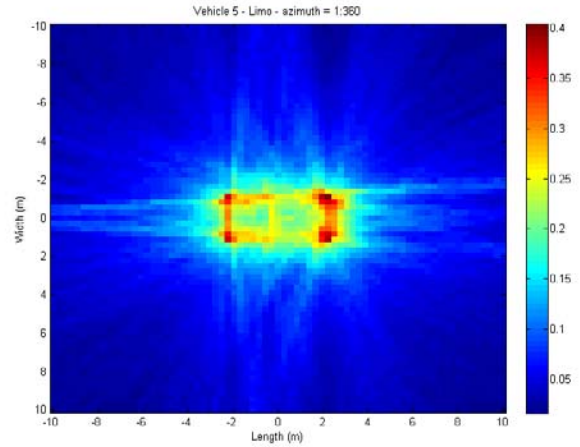


Figure 7 - Back-Projection Imagery

6. TARGET RECOGNITION

To perform target recognition on the In SAR imagery, we computed the Euclidean distance between each template (pre-confusion) and test (post-confusion) image (after a Matrix 2-Norm normalization step). For each test case, we computed the template image for all 20 vehicles, and computed the test image for all 20 vehicles. The results were stored in an error matrix. Figure 8 shows the error matrix for one of the test cases. Through initial testing, it was found that the Euclidean distance metric was equally as effective as the correlation peak method in our 20 vehicle classification problem, thus our tests were all conducted with the Euclidean distance metric.

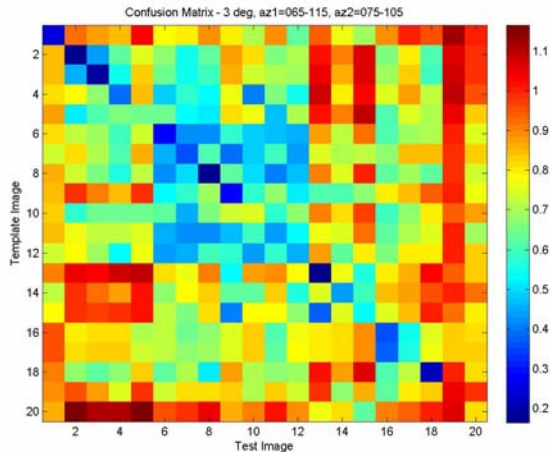


Figure 8 - Error Matrix

7. RESULTS

For our 20-vehicle classification problem we defined a “detection” as a correctly classified target, and a “false-alarm” as a classification to any other target. Thus, given an error matrix \mathbf{C} , we computed P_D and P_{FA} for a given threshold k as:

$$P_D = \frac{1}{N} \sum_{i=1}^N \mathbf{1}(C_{i,i} < k), \quad (36)$$

$$P_{FA} = \frac{1}{N^2 - N} \sum_{i=1}^N \sum_{j=1}^N \mathbf{1}(C_{i,j} < k) \mathbf{1}(i \neq j). \quad (37)$$

where $\mathbf{1}(\cdot)$ is the indicator function and $\mathbf{C}_{i,j}$ is the i,j^{th} element of the error matrix. We tested our back-projection imaging algorithm on four different test cases, shown in Table I, designed to mimic real-world scenarios that a multi-aircraft tracking system would face. For each test case, the ROC curve is computed for elevation angles of 3° , 5° , 7° , and 9° . The XPATCH data was collected with a separation of 1° between azimuth samples. We also computed the ROC curve for a classifier that utilizes the estimated target dimensions for recognition. The results for the three of the ten test cases are shown in Figures 9-15.

Table I - Test Cases

	Test Case	Pre-Confusion	Post-Confusion
1	Front/Rear Asymmetric	$0^\circ:30^\circ$	$180^\circ:210^\circ$
2	Front/Rear Non-Contiguous	$-30^\circ:30^\circ$	$150^\circ:210^\circ$
3	Partially Overlapping (F)	$-25^\circ:25^\circ$	$0^\circ:45^\circ$
4	Separated Patches (F)	$-15^\circ:15^\circ$	$30^\circ:60^\circ$

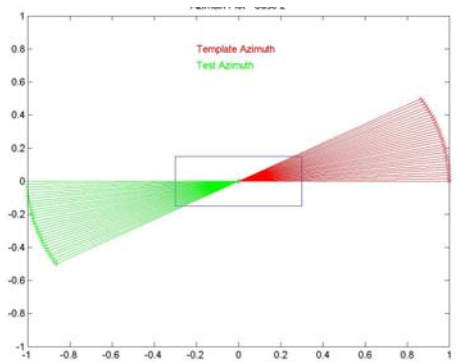


Figure 9 - Case 1 - Azimuth Plot

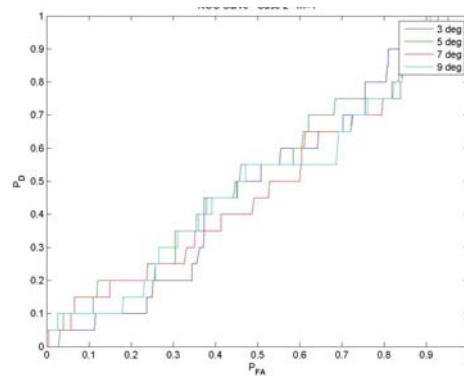


Figure 10 - Case 1 - ROC Curve

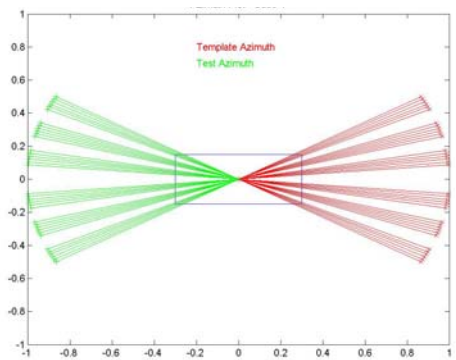


Figure 11 - Case 2 - Azimuth Plot

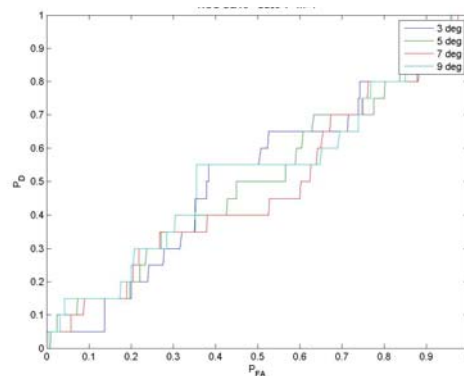


Figure 12 - Case 2 - ROC Curve

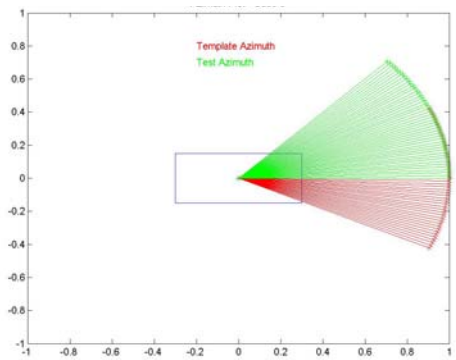


Figure 13 - Case 3 - Azimuth Plot

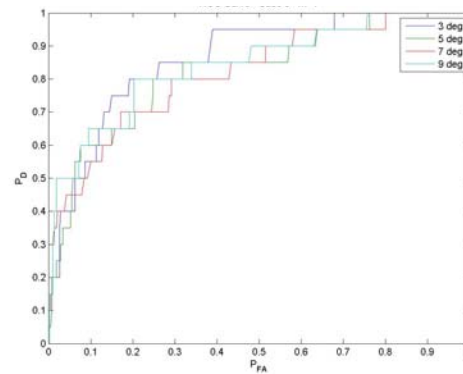


Figure 14 - Case 3 - ROC Curve

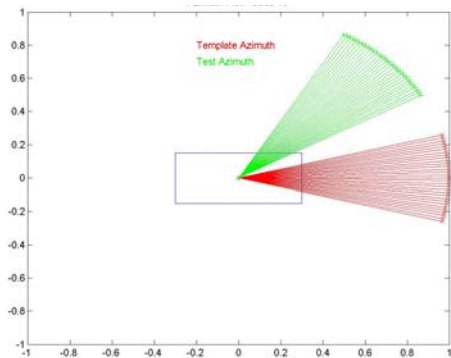


Figure 15 - Case 4 - Azimuth Plot

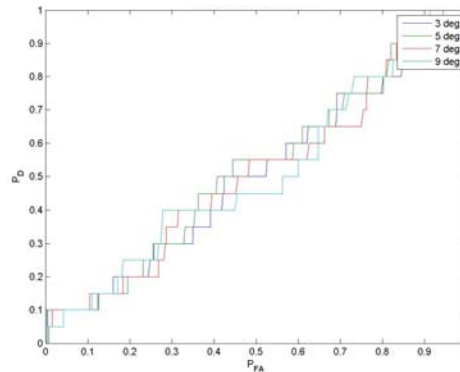


Figure 16 - Case 4 - ROC Curve

8. CONCLUSION

In this paper, we presented the derivation of our EA-InSAR image formation algorithm for HRR profile libraries. We tested the viability of using the generated images for target recognition/classification, as opposed to using direct comparisons of the profiles themselves.

Our tests were run with XPATCH data on a class of 20 different test vehicles of varying size, but there are several more tests that would be informative to run. Foremost, the assumption that a vehicle's HRR profile may be completely isolated is not realistic. To more fully characterize the performance of our method it would be advisable to devise simulations that include secondary objects as coherent noise sources, such as a nearby vehicle that is present at some or all azimuth angles, since a trailing vehicle in a convoy may distort the HRR profile for some azimuth angles, especially if the template is constructed without such interference.

Armed with the target identification capability that EA InSAR provides, system developers can readily incorporate this classification method into feature-aided tracking algorithms [3,4,8] for increased performance. The ability to process HRR data that does not have any pre and post confusion overlap is an advantage of our EA InSAR algorithm clearly provides.

APPENDIX

Table II - Test Vehicles

Number	Description	L (m)	W (m)
1	HMMWV	4.622	2.754
2	Blazer	4.798	2.627
3	Chevy Pickup	5.480	2.627
4	BRDM-2	5.890	2.328
5	Mercedes Limo	6.002	2.014
6	M-35 Truck	6.718	2.499
7	BMP-2	6.748	3.158
8	MLRS	6.956	3.300
9	BMP-3	7.030	3.040
10	BTR-70	7.624	2.822
11	ZIL-131 Truck	7.650	2.709
12	2S6 Tunguska	7.831	3.274
13	M-109	8.986	3.174
14	LAV-25	9.231	3.423
15	T-62 Tank	10.000	3.374

16	Empty Scud TEL	11.476	2.946
17	Scud TEL w/missile down	11.476	2.946
18	Schoolbus	11.614	3.226
19	Smerch	11.784	3.098
20	Tanker Truck	15.550	2.600

ACKNOWLEDGMENT

The authors would like to thank Lucien Tieg and David Choi for their valuable consultation and for providing the simulation data which was utilized to develop and test this algorithm.

REFERENCES

- [1] Chen, J. S., and Walton, E. K., "Comparison of two target classification techniques," IEEE Transaction on Aerospace and Electronic Systems, vol. 22, no. 1, Jan. 1986, pp. 15-21.
- [2] Chong, C.-Y., Garren, D., and Grayson, T., "Ground Target Tracking – a Historical Perspective," in Proc. Of 2000 IEEE Aerospace Conf., Vol. 3, 18-25 March 2000, pp. 433 – 448.
- [3] Chong, C.-Y., Mori, S., "Metrics for Feature-Aided Track Association," in Proc. Of 9th Int'l Conf. on Information Fusion (ICIF '06), July 2006.
- [4] Ehrman, L.M., Blair, W.D., "Comparison of methods for using target amplitude to improve measurement-to-track association in multi-target tracking," in Proc. Of 9th Int'l Conf. on Information Fusion (ICIF '06), July 2006.
- [5] Jacobs, S. P., "Automatic Target Recognition using High Resolution Radar Range-Profiles," PhD. Thesis, Washington University, Saint Louis, MO, May 1997.
- [6] Jacobs, S. P., and O'Sullivan, J. A., "Automatic Target Recognition Using Sequences of High Resolution Radar Range-Profiles," IEEE Transactions on Aerospace and Electronic Systems, vol. 36, no. 4, April 2000, pp. 364-382.
- [7] Ksienski, A. A., Lin, Y.-T., and White, L. J., "Low-Frequency Approach to Target Identification," Proceedings of the IEEE, vol. 63, no. 12, Dec. 1975, pp. 1651-1659.
- [8] Ruan, Y., Hong, L., "Feature-aided tracking with GMTI and HRR measurements via mixture density estimation," IEE Proc. On Control Theory and Applications, Vol. 153, Iss. 3, 9 May 2006, pp. 342 – 356.
- [9] Tait, Peter, Introduction to Radar Target Recognition, Institution of Electrical Engineers, 2005.